JOURNAL OF APPLIED ELECTROCHEMISTRY 11 (1981) 703–713

Kinetics of the polycrystalline iron electrode in dilute acid and neutral aqueous electrolytes under complex fast potentiodynamic perturbations

J. O. ZERBINO, J. R. VILCHE, A. J. ARVÍA

Instituto de Investigaciones Fisicoquímicas Teóricas y Aplicadas (INIFTA), División Electroquímica, Sucursal 4, Casilla de Correo 16, 1900 La Plata, Argentina

Received 6 January 1981

The potentiodynamic response of the polycrystalline Fe electrode in aqueous electrolytes containing K_2SO_4 ($2 \leqslant pH \leqslant 7$) under fast perturbation conditions is investigated. When the conditions are properly adjusted, film-forming species and an oxide phase are detected. The results obtained by the application of the triangularly modulated triangular potential sweep (TMTPS) technique show the degree of reversibility of the various anodic and cathodic processes related to the electrodissolution of iron. The experimental response can be interpreted through a complex reaction model involving electrochemical reactions and ageing processes. The model contains, as particular cases, most of the mechanisms proposed earlier for the dissolution of iron in aqueous solution. The electrochemical interface is conceived as dynamic, deprotonation and dehydration processes playing an important role during the Fe electro-oxidation.

1. Introduction

The corrosion of iron and its passivation in aqueous solutions have been the subject of special attention for a long time, but, despite the large amount of data reported, the mechanistic interpretation of the processes is still under discussion, as can be seen in the most recent publications [1–14]. The potentiodynamic polarization of iron in 10% Na_2SO_4 at low sweep rates shows the characteristic features of anodic dissolution and passivation [14]. Oxide removal is observed during negative-going potential sweeps [13–16] and two anodic dissolution current peaks are found with clean electrode surfaces. The number of anodic current peaks depends on the presence of oxide on the surface and on the potential sweep rate. It is well accepted that the kinetics of the corrosion process involves a complex reaction mechanism, and thus has been discussed particularly for electrolytes at pH values lower than 3 [17–24]. On the other hand, both in the intermediate pH range and at pH higher than 10, the models proposed to interpret the reactions are more limited. Nevertheless, there is some evidence that the processes over the whole potential range may be described by a more general reaction pathway [25].

To establish the likely reaction mechanism of the iron electrode in aqueous solutions, it is necessary to study the participation and stability of various electrosorbed or film-forming species in the metal electro-oxidation reaction. Most of the reaction mechanisms postulated for the iron electrode imply the existence of various species whose structure and properties depend both on the electrolyte composition and on the potential perturbation applied to the electrode. There is evidence that the electrodissolution mechanism shows an apparent change at a critical pH value of approximately 3.5 [12, 25]. In this respect, the present paper deals with the response of the iron electrode in the pH range from the critical pH up to neutrality. The aim of this study is to determine the behaviour of the iron electrode under relatively fast potentiodynamic perturbations (either simple or complex) and to gain information about the participation of film-forming species in the electrodissolution process.

0022–891X/81/060703–11$03.10/0

2. Experimental method

The Fe/xN H_2SO_4 + yN K_2SO_4 interphase ($0 \leqslant x \leqslant 10^{-2}$ and $0.49 \leqslant y \leqslant 0.50$) consisted of a polycrystalline iron wire (Johnson Matthey Chemicals Ltd) of specpure quality, 0.05 cm in diameter and of 0.25 cm^2 apparent area, immersed in aqueous solutions prepared from analytical reagent-grade chemicals, (pa Merck) and triply distilled water. The solution was N_2-saturated before each run and kept continuously under N_2 gas at 25° C. The iron electrodes were mechanically polished with emery paper of different grades and with a fine-grade alumina–acetone suspension. Before each potentiodynamic measurement the electrode was held for 5 min in the hydrogen evolution potential region. The electrochemical cell, the rest of the equipment and general procedures were the same as already described in previous papers [26–28]. The electrode potentials are referred in the text to the normal hydrogen electrode.

The electrochemical interface was subjected to several potential profiles, namely (a) repetitive triangular potential sweeps (RTPS) at potential sweep rates (v) of between 0.1 and 50 V s^{-1} within fixed cathodic ($E_{s,c}$) and anodic ($E_{s,a}$) switching potentials; (b) RTPS with either $E_{s,c}$ or $E_{s,a}$ fixed and stepwise changing of the other limit and (c) triangularly modulated triangular potential sweeps (TMTPS) [28–30] with different base signal sweep rates (0.2 V $s^{-1} \leqslant v_b \leqslant$ 20 V s^{-1}), different modulating signal sweep rates (5 V $s^{-1} \leqslant v_m \leqslant$ 100 V s^{-1}) and different amplitude of the modulating signal (0.03 V $\leqslant \Delta E_m \leqslant$ 0.18 V).

3. Results

3.1. *The Fe/0.5N K_2SO_4 interphase*

The conventional RTPS E–I displays run with 0.5N K_2SO_4 at 0.3 V s^{-1} depend on the potential cycling conditions. Thus, for those runs between − 1.10 V and − 0.50 V (Fig. 1a), the overall charge decreases gradually from the first TPS to attain a stable value after about 20 cycles. The charge of the first anodic current peak in the stabilized E–I profile is near 0.7 mC cm^{-2}, a figure which is close to that for metal (II) hydroxide monolayers [31, 32]. The stabilized profile

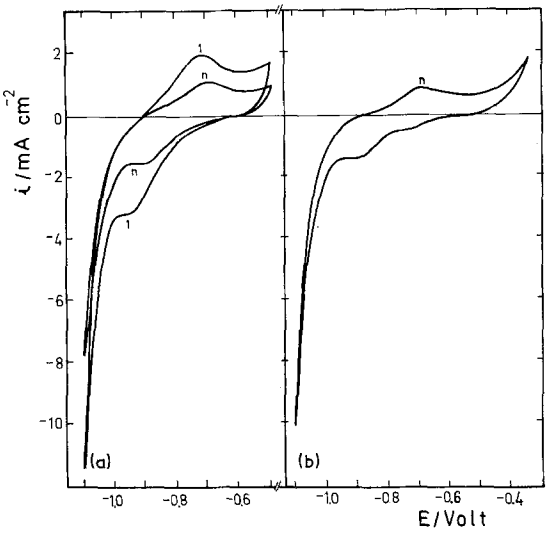

Fig. 1. Potentiodynamic E–I contours obtained in 0.5 N K_2SO_4 at 0.3 V s^{-1}. (a) The 1st and nth profiles run with RTPS between − 1.10 V and − 0.50 V. (b) Stabilized E–I profile run with RTPS between − 1.10 V and − 0.35 V, v = 0.3 V s^{-1}.

involves a broad anodic current peak preceding the metal electrodissolution and a cathodic shoulder preceding the hydrogen evolution. A poorly defined cathodic current peak results when $E_{s,a}$ is extended to − 0.33 V (Fig. 1b). The characteristics of the E–I display, however, are different when $E_{s,c}$ = − 1.10 V and $E_{s,a}$ = − 0.20 V (Fig. 2). Then, the overall charge increases remarkably during potential cycling, the cathodic current peak at − 0.77 V becomes clearly defined and the corresponding limiting charge is close to 13 mC cm^{-2}. The charge increase occurring at positive potentials is associated with the metal electrooxidation reaction. It is similar to that which would be observed if a porous film of oxide/hydroxide with more than one possible oxidation state were growing with time. However, in the potential range of the present experiments, this contribution to the charge increase seems to be less important than the metal electrodissolution to a Fe(II) film-forming species.

When $E_{s,c}$ = − 0.95 V and $E_{s,a}$ = − 0.20 V, the change of the E–I profile during the RTPS apparently involves a progressive depolarization of the electrodissolution reaction and an increasing polarization of the hydrogen evolution reaction. Simultaneously a cathodic current peak at − 0.78 V and a shoulder at − 0.88 V are noticed.

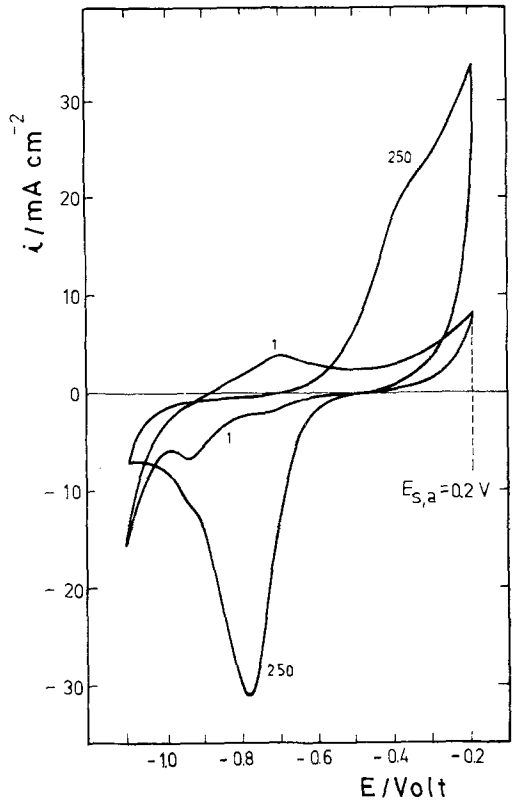

Fig. 2. Potentiodynamic E–I contours corresponding to the 1st and 250th potential cycles obtained with RTPS in 0.5 N K_2SO_4, $v = 0.3$ V s^{-1}; $E_{s,c} = -1.10$ V and $E_{s,a} = -0.20$ V.

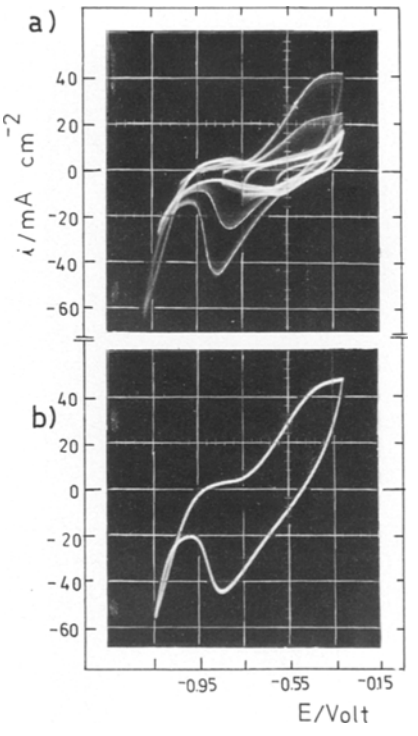

Fig. 3. Influence of the cathodic switching potential on the potentiodynamic I–E contour at 20 V s^{-1} in 0.5 N K_2SO_4. $E_{s,a} = -0.31$ V. (a) Each full trace was recorded by changing $E_{s,c}$ from -0.60 V to -1.25 V after ten potential cycles. (b) RTPS I–E profile run between -1.17 V and -0.31 V.

The charge decrease of the cathodic current peak depends on the preset $E_{s,c}$ value.

Conventional RTPS at 20 V s^{-1} with gradually changing $E_{s,c}$ (Fig. 3a) or $E_{s,a}$ allow the definition of the potential range associated with each current peak. Accordingly, as $E_{s,c}$ moves step-wise towards more negative potentials, the cathodic current peak at about -0.59 V is observed. For the latter no conjugated anodic current peak is recorded, but its occurrence is associated with an apparently irreversible process related to metal electrodissolution. Otherwise, when $E_{s,c}$ is more negative than -0.85 V, a broad cathodic asymmetric peak at about -0.85 V is recorded. This is related to the anodic current plateau extending into the -0.45 to -0.30 V region. Finally, when $E_{s,c}$ is more negative than -0.95 V, there is a clear cathodic contribution by the hydrogen evolution reaction as well as a possible contribution by the hydrogen electro-oxidation this is reflected through the small anodic hump located in the -0.95 V to -0.85 V range. Furthermore, the anodic current peak formerly located at about -0.7 V is now recorded at about -0.45 V. The occurrence of broad anodic and cathodic current peaks should be related in part to changes in local pH at the reaction interface, and in part to the ability of the growing porous film to charge and discharge.

The corresponding TMTPS E–I contours, run under the conditions indicated in Fig. 4, show different characteristics depending on whether the positive-going potential (PGPS) or the negative-going potential (NGPS) scan is considered. A reasonable fine structure for the E–I displays can be obtained by selected TMTPS perturbation conditions (Figs. 4b and c). The PGPS shows the irreversible contribution of the hydrogen electro-oxidation at roughly -0.85 V and a coupled redox reaction in the -0.70 V to -0.50 V range. The anodic contribution of the latter appears as a hump at the left-hand side of the overall asym-

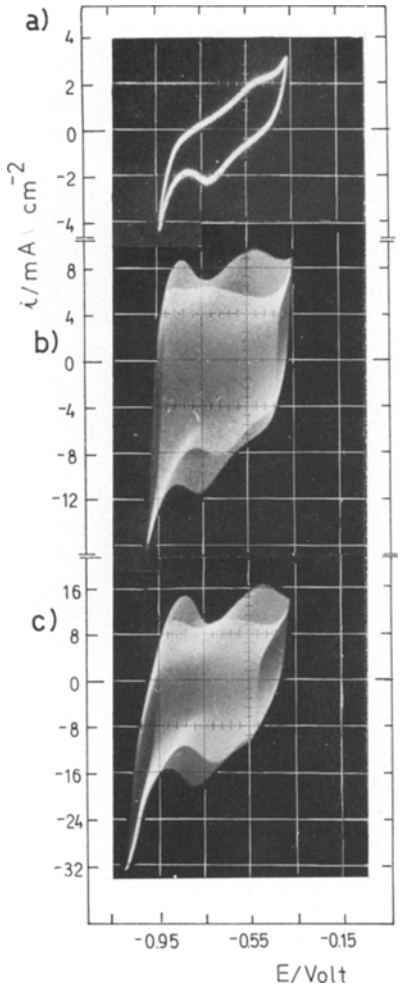

Fig. 4. Comparison between RTPS and TMTPS voltammograms in 0.5 N K_2SO_4. (a) $v = 2$ V s^{-1}; (b) $v_b = 2$ V s^{-1}, $v_m = 100$ V s^{-1}, $\Delta E_m = 0.09$ V; (c) $v_b = 2$ V s^{-1}, $v_m = 100$ V s^{-1}, $\Delta E_m = 0.18$ V.

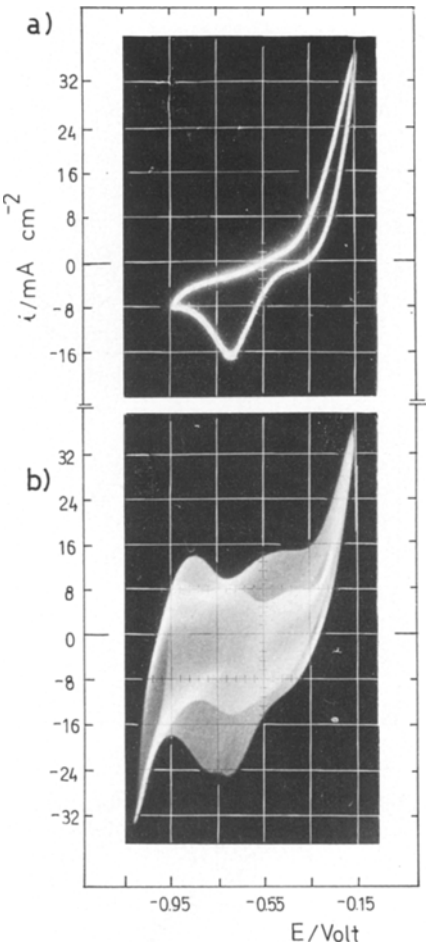

Fig. 5. Comparison between RTPS and TMTPS voltammograms in 0.5 N K_2SO_4. (a) $v = 2$ V s^{-1}; (b) $v_b = 2$ V s^{-1}, $v_m = 100$ V s^{-1}, $\Delta E_m = 0.18$ V.

metric current peak recorded at about − 0.45 V. This peak precedes the appearance of an irreversible third process taking place at potential close to $E_{s,a}$. The NGPS shows the same contributions as the PGPS but the location of the peaks and their relative current distributions are appreciably different from those already described because of the complex kinetics of the overall reaction.

The above description also depends on the values of both $E_{s,c}$ and $E_{s,a}$ (Fig. 5). When $E_{s,a}$ becomes more positive there is a clear accumulation of charge which manifests itself in the electroreduction process and, simultaneously, a clear shift and splitting of the NGPS cathodic envelope are observed. These reveal possible structural changes of the species formed during the anodic process.

3.2. *The $Fe/10^{-4}N\ H_2SO_4 + 0.5N\ K_2SO_4$ interphase*

The *E–I* displays obtained with 10^{-4} N H_2SO_4 + 0.5N K_2SO_4 solutions are similar to those already described for the 0.5N K_2SO_4 solution. The profiles of the conjugated couples are shifted towards more positive potentials in going from the neutral to the acid electrolyte. For the cathodic processes at pH > 4 the *E–I* RTPS displays obtained under stirring are to some extent simpler than those run with still solutions. No influence of stirring is

observed in the metal electrodissolution potential range, excepting the anodic plateau preceding this reaction. The stirring tends to conceal the hydrogen ion concentration gradient at the metal solution interface, produced particularly by the hydrogen evolution reaction at the negative potential side and by the hydrolysis of the electrodissolution products at the positive potential side. Therefore, the influence of stirring is associated with the chemical dissolution of the oxo-hydroxide films which are formed at the metal/solution interface during the anodic process.

3.3. *The Fe/10^{-3}N H_2SO_4 + 0.499N K_2SO_4 interphase*

As the pH decreases from ~ 7 to ~ 3 the *E–I* displays run at 20 V s^{-1} (Figs. 6 and 7) show an increase of the anodic contribution preceding the electrodissolution reaction. The anodic contribution defines a net anodic current peak at − 0.47 V when $E_{s,c} < -1.15$ V. Simultaneously, two clear cathodic current peaks are distinguished in the − 0.65 V to − 0.95 V range, whose relative contributions depend upon $E_{s,c}$ and $E_{s,a}$. These cathodic current peaks are well formed when $E_{s,a} < -0.15$ V. On the other hand, the complex anodic current peak at − 0.95 V is related to the hydrogen evolution reaction, while the cathodic current peak located at less negative potentials is related to the processes preceding the electrodissolution of the metal. The charge estimated for the latter is of the order of 0.6 mC cm^{-2}.

The splitting of the cathodic *E–I* contour is

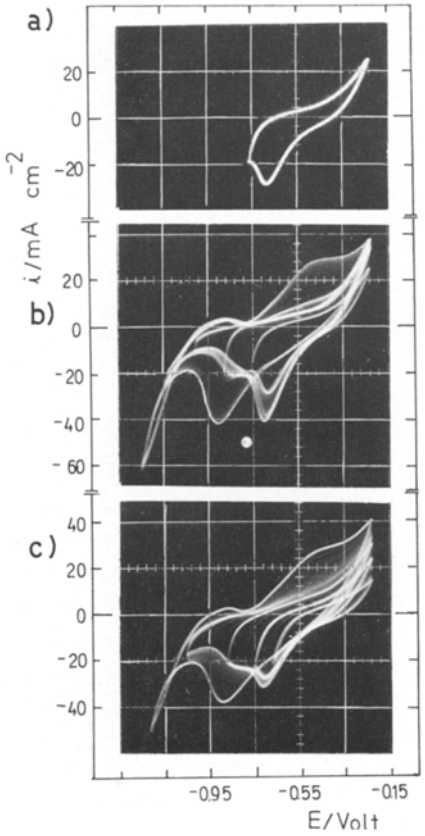

Fig. 6. Influence of the cathodic switching potential on the potentiodynamic *I–E* contour at 0.2 V s^{-1} in 10^{-3} N H_2SO_4 + 0.499 N K_2SO_4 solution; $E_{s,a} = -0.23$ V. (a) RTPS *I–E* profile between − 0.75 V and − 0.23 V. (b) Each full trace was recorded by stepwise decrease of $E_{s,c}$ after ten potential cycles. (c) Each run was made by stepwise $E_{s,c}$ increase once the RTPS conditions described above had been attained.

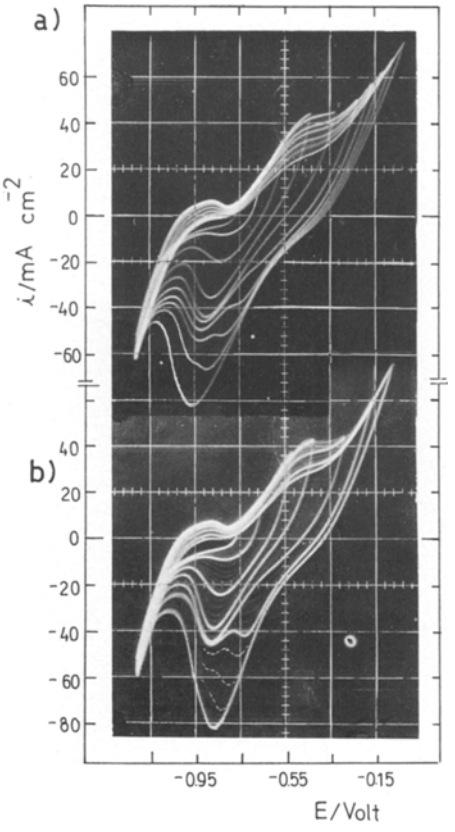

Fig. 7. Influence of the anodic switching potential on the potentiodynamic *I–E* contour at 20 V s^{-1} in 10^{-3} N H_2SO_4 + 0.499 N K_2SO_4 solution; $E_{s,c} = -1.20$ V. (a) Each run was made after attaining the stabilized *E–I* profile between − 1.20 V and − 0.03 V by decreasing $E_{s,a}$ stepwise and recording at the 10th cycle. (b) Each run was made by changing $E_{s,a}$ stepwise from − 0.75 V up to − 0.03 V and recording *E–I* at the 10th cycle.

also produced by running *E–I* displays with either stepwise decrease and increase of $E_{s,c}$ or stepwise increase and decrease of $E_{s,a}$ (Figs. 6 and 7). The stabilized *E–I* displays depicted in the figures with full traces result after about 10 RTPS between $E_{s,c}$ and $E_{s,a}$. As $E_{s,c}$ becomes more negative, the height of the cathodic current peak at -0.7 V decreases and the heights of the cathodic current peak at -0.9 V, the anodic current peak at -0.45 V, and the current plateau at about -0.90 V increase (Figs. 6a and b). The opposite effects are observed when $E_{s,a}$ moves stepwise towards more positive potentials.

Similar changes of the *E–I* displays can be obtained by holding the potential at $E_{s,c}$ for different times τ (10^{-4} s $\leqslant \tau \leqslant 10^{-1}$ s) (Fig. 8). At $E_{s,c} = -0.97$ V a net electroreduction process together with hydrogen evolution takes place. These results demonstrate that the extent of the anodic process undergone within the -0.96 V to -0.40 V range strongly depends on the degree of electroreduction of the metal surface achieved during the negative-going potential scan.

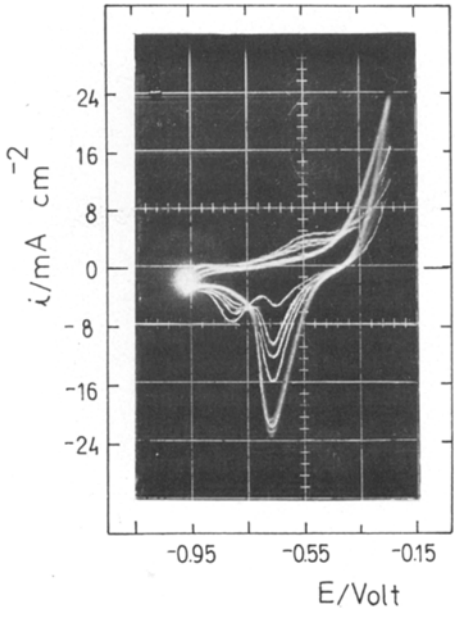

Fig. 8. Comparison between the RTPS voltammogram run at 2 V s^{-1} in 10^{-3} N H_2SO_4 + 0.499 N K_2SO_4 solution between -0.97 V and -0.23 V and STPS *E–I* displays run at 2 V s^{-1} after holding the potential at $E_{s,c}$ for the time τ, for $\tau = 10^{-4}$ s, 10^{-3} s, 10^{-2} s and 10^{-1} s.

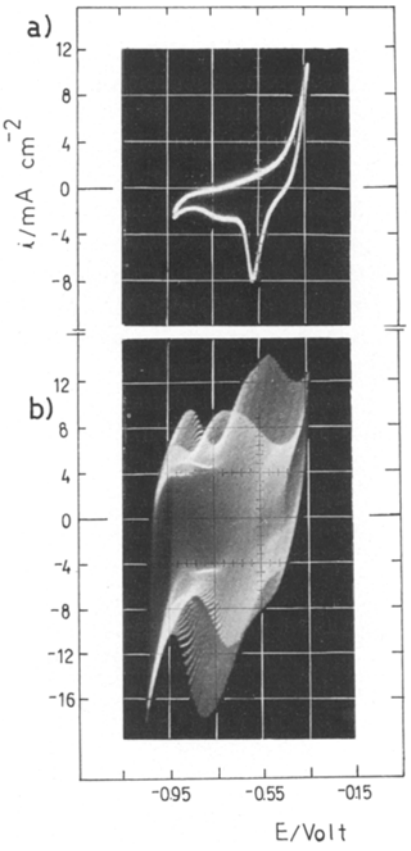

Fig. 9. Comparison between RTPS and TMTPS voltammograms in 10^{-3} N H_2SO_4 + 0.499 N K_2SO_4 solution. (a) $v = 2$ V s^{-1}; (b) $v_b = 2$ V s^{-1}, $v_m = 50$ V s^{-1}, $\Delta E_m = 0.135$ V.

The TMTPS *E–I* displays (Figs. 9 and 10) reveal the same current contributions already described at higher pH. The cathodic current related to the process occurring at more positive potentials overlaps with that of the conjugated couple lying in the -0.7 V to -0.5 V range. This conjugated couple is only observed when $E_{s,c} < -1.0$ V or when the potential is held at $E = -0.9$ V for the time τ (Fig. 8). The corresponding anodic to cathodic peak potential differences ($\Delta E_p = 0.09$ V) both in the NGPS and in the PGPS are practically coincident and the charge involved, which is in the order of 0.65 mC cm^{-2}, shows a pseudocapacitive behaviour (Fig. 6) [33–35]. The reaction taking place at more positive potentials is slower than that of the conjugated couple found at lower potential values (Fig. 10).

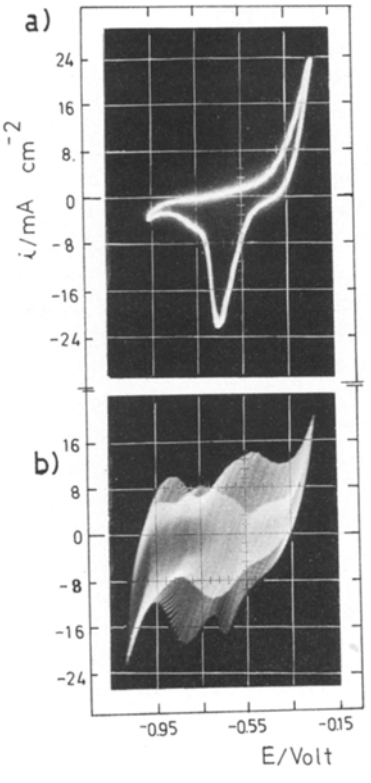

Fig. 10. Comparison between RTPS and TMTPS voltammograms in 10^{-3} N H_2SO_4 + 0.499 N K_2SO_4. (a) v = 2 V s^{-1}; (b) v_b = 2 V s^{-1}, v_m = 50 V s^{-1}, ΔE_m = 0.135 V.

3.4. *The $Fe/10^{-2}N\ H_2SO_4 + 0.49N\ K_2SO_4$ interphase*

The potentiodynamic E–I displays at $E >$ − 0.45 V exhibit a net anodic current which increases rather abruptly in the range − 0.3 V to 0 V, the potential range usually assigned to the active electrodissolution of iron [17–25]. At the highest potentials the E–I profile obtained during the positive-going potential sweep almost coincides with that of the returning potential scan. The separation of both E–I profiles in the − 0.3 V to − 0.5 V range is attributed to the double-layer charging and discharging. On the other hand, the E–I profiles recorded at $E <$ − 0.45 V involve only cathodic currents which are associated with the hydrogen evolution reaction. This portion of the E–I displays is extremely sensitive to both $E_{s,c}$ and $E_{s,a}$. The stepwise increase of $E_{s,c}$ during the successive potential scans produces a remarkable change of the E–I profile in which the cathodic current decreases from a well-defined current peak to a smaller limiting current as $E_{s,c}$ becomes more negative. This change can be related to the gradual local increase in pH due to the increasing hydrogen evolution as $E_{s,c}$ becomes more negative.

After changing $E_{s,a}$ stepwise from more positive to more negative values or vice versa, the changes in the hydrogen evolution region are the same as already described, except that in this case, because of the preset perturbation conditions, a remarkable increase of the iron electrodissolution current is noticed as the local pH increases. Similarly, at relatively large v the main cathodic current peak, which is related to the hydrogen evolution reaction, manifests itself as a complex current peak involving at least two distinguishable contributions preceding the hydrogen evolution. Furthermore, the E–I displays tend to depict a cathodic current contribution at around − 0.35 V during the negative-going potential excursion. The latter is definitely established after perturbing the electrode with the TMTPS perturbation programme.

The TMTPS E–I contours run either towards positive or towards negative potentials and exhibit a broad cathodic current peak in the potential range preceding the proper metal electrodissolution. Within this potential range the fast response of the modulating signal indicates that besides the double-layer charging and discharging there is also a small pseudocapacitance contribution which might be associated with an electrochemical stage preceding the complete electro-oxidation of the metal.

Both the PGPS and NGPS show an anodic current peak at − 0.9 V which is apparently part of the conjugated couple related to the hydrogen evolution reaction. Furthermore, the NGPS exhibits an additional cathodic current peak at about − 0.92 V which is not observed in the PGPS. The latter coincides with the cathodic current peak related to the hydrogen ion discharge.

4. Interpretation and discussion

The kinetics of the anodic dissolution of iron in aqueous electrolytes at pH in the vicinity of neutrality, is apparently more complicated than

in acid solutions at pH < 2 or in alkaline solutions at pH > 10. The complication in part arises because of the abrupt change of local pH during the faradaic processes, which obviously depends on the magnitude and type of potential perturbation applied to the electrode, and the hydrolysis of metal ions in solution. Consequently, the interpretation of the electrochemical measurements is relatively more difficult due to the fact that the coverage of the metal surface with oxygen-containing species, either electrosorbed or produced during the anodic reaction, increases strongly with the increasing pH value. Furthermore, the formation of tridimensional oxygen-containing layers takes place in the prepassive region. The behaviour of these layers is time dependent due to the so-called ageing effects [33], which were observed in alkaline electrolytes at pH greater than 10 [27, 34]. The ageing effects can, however, be minimized to some extent through potentiodynamic runs made with fast potential sweep rates so that the amount of charge involved approaches that of a mono- or submonolayer.

From this theory of electrochemical reactions under TMTPS [35, 36] one can envisage some qualitative aspects of the complex electrochemical reactions. The TMTPS experiments show that at least two redox systems are formed at the iron surface along the potential scan and that the electrodissolution process takes place through the surface film, which under the perturbation conditions used is of the order of one monolayer thick, or thereabouts. On the other hand, apart from the change of the *E–I* profiles due to the local pH value, they exhibit potential peak shifts which can be associated with the ageing of the film formed on the electrode surface.

The TMTPS response fits a formal reaction pattern involving at least two electron transfer processes coupled to chemical reactions of the different surface species [35, 36]. Therefore, the simplest basic formalism of the overall process related to the iron electrode is as follows:

$$A \underset{k_{-1}}{\overset{k_1}{\rightleftharpoons}} B + e \qquad (1)$$

$$B \underset{k_{-2}}{\overset{k_2}{\rightleftharpoons}} C + e \qquad (2)$$

$$C \xrightarrow{k_3} C^* \xrightarrow{k_{-3}} B \qquad (3)$$

where A is the reactant and B, C and C* are surface species and k_i and k_{-i} are the corresponding specific rate constants for the forward and backward reactions respectively. This reaction sequence explains the features of the TMTPS *E–I* profiles (Figs. 4, 5, 9 and 10) if Step 3, which corresponds to the ageing of one of the surface species, is a slow step; that is, if $k_{-3} \ll k_{-2}$ [35, 36]. This means that the species C* requires a larger electroreduction overvoltage than species C. Therefore, the modulating (NPGS) signal obtained in the − 0.65 V to − 0.85 V potential range should correspond to Reaction 1.

The shift of the corresponding electroreduction current peak towards more negative potentials appears as a consequence of the ageing process. The latter increases to some extent the irreversibility of the electroreduction process associated with Step 1. Otherwise, the conclusion about the reversible characteristics of Step 1 is in agreement with most of the reaction mechanisms postulated for the electrodissolution of iron in acid solutions [18–21].

The interpretation of the redox couple lying in the − 0.85 V to − 0.45 V potential range is based on Steps 1–3. In the case of Step 2, in order to explain the ageing effect of the corresponding electroreduction current peak, it should be admitted that species B also suffers ageing, according to:

$$B \xrightarrow{k_4} B^* \xrightarrow{k_{-4}} A. \qquad (4)$$

This possibility is difficult to elucidate because the corresponding electrochemical response probably overlaps those of Steps 2 and 3; that is, $k_{-1} > k_{-4} \gtrsim k_{-2} > k_{-3}$. The redox couple recorded in the − 0.85 V to − 0.45 V range can be associated with a surface reaction involving the transfer of two electrons coupled to the ageing process. The contribution of this redox couple appears clear when the iron electrode is cathodized at $E < -0.96$ V and the anodic potential limit is lower than − 0.35 V (Fig. 7).

The species B and C participate in electrooxidation processes occurring at more positive potential, yielding the final product (S) in solution:

$$B \rightarrow S + e \qquad (5)$$

and

$$C \rightarrow S + e\,. \qquad (6)$$

Reactions 5 and 6 can be related to the redox

E–I profile observed in the -0.70 V to -0.15 V range. Depending on pH and applied potential the soluble ions in solution eventually participate either in the hydrolysis equilibrium reactions and/or the hydroxide film growth.

The cathodic charge associated with the redox couple located in the -0.70 V to -0.10 V range decreases with $E_{s,a}$ (Fig. 7) and correspondingly the overall cathodic current peak potential shifts towards more positive potentials. Then, under these conditions, the electrochemical reaction related to the formation of the hydroxide phase becomes more reversible and there is an increase in the couple signal related to Reactions 1–3.

The existence of the redox couple associated with Reactions 5 and 6 adds a further complication to the reaction mechanism. However, its contribution in the overall reaction, as far as its charge contribution in the TMTPS experiments is concerned, becomes relatively low. Because of this fact and also because of the uncertainty of the corresponding kinetic parameters, its contribution in the present interpretation of the process is disregarded.

On the basis of the proposed formal reaction scheme, the characteristics of the potential perturbation should play a definite role in establishing the contribution ratio of both redox couples in the overall response of the electrochemical reaction (Figs. 6 and 7). The reaction formalism can be correlated with the possible species which are usually assigned to the anodic dissolution of iron in aqueous solutions in the absence of O_2 and surface-active substances. The explicit anodic dissolution mechanism can, therefore, be put forward as follows.

(a) Formation of the first layers:

$$\{Fe\}[Fe(H_2O)] \rightleftharpoons \{Fe\}[Fe(OH)] + H^+ + e \quad (7)$$

$$\{Fe\}[Fe(OH)] \rightleftharpoons \{Fe\}[Fe(OH)_2] + H^+ + e. \quad (8)$$

(b) Ageing of the surface species:

$$\{Fe\}[Fe(OH)_2] \longrightarrow \{Fe\}[Fe(OH)_2]^* \quad (9)$$

$$\{Fe\}[Fe(OH)] \longrightarrow \{Fe\}[Fe(OH)]^* \quad (10)$$

(c) Base metal electrodissolution:

$$\{Fe\}_x[Fe(OH)] + H_2O \longrightarrow \{Fe\}_{x-1}[Fe(H_2O)] + FeOH^+ + e \quad (11)$$

$$\{Fe\}_x[Fe(OH)_2] + H_2O \longrightarrow \{Fe\}_{x-1}[Fe(OH)_2] + FeOH^+ + H^+ + 2e \quad (12)$$

$$\{Fe\}_x[Fe(OH)]^* + H_2O \longrightarrow \{Fe\}_{x-1}[Fe(H_2O)] + FeOH^+ + e \quad (13)$$

$$\{Fe\}_x[Fe(OH)_2]^* + H_2O \longrightarrow \{Fe\}_{x-1}[Fe(OH)_2] + FeOH^+ + H^+ + 2e. \quad (14)$$

(d) Oxide phase formation:

$$\{Fe\}_{x-n}[Fe(OH)_2] + H_2O \longrightarrow \{Fe\}_{x-i}[Fe(II)\text{–hydrated hydroxide}] + H^+ + e \quad (15)$$

$$[Fe(II)\text{–hydrated hydroxide}] \longrightarrow [Fe(III)\text{–oxyhydroxide}] + H_2O + H^+ + e. \quad (16)$$

(e) Hydrolysis equilibria:

$$H^+ + FeOH^+ \rightleftharpoons Fe^{2+} + H_2O \quad (17)$$

$$FeOH^+ + H_2O \rightleftharpoons Fe(OH)_2 + H^+ \quad (18)$$

where the braces denote a bulk phase, the brackets correspond to a product formed on the metal surface and the parentheses indicate adsorbed species. The metal electrodissolution reaction may occur through either $[Fe(OH)]$, $[Fe(OH)_2]$, $[Fe(OH)]^*$ or $[Fe(OH)_2]^*$ species.

The steps in the reaction model can be grouped in the following way. Consecutive steps (Steps 7, 11 and 17) are formally equivalent to the Bockris mechanism [18] for the anodic dissolution of iron in acid electrolytes and Steps 7 and 12 can be related to the catalytic mechanism postulated by Heusler [17]. These reaction pathways where anion adsorption is neglected should predominate at $pH < 3$, as recently reported by Lorenz [12]. Steps 7–10 indicate reactions associated with the O-containing surface layers operating more clearly at $pH > 4$. The dissolution of the base metal through the different film-forming species is feasible, but this depends on the film thickness and, for thick films (> 5 nm), on the film conduction characteristics [37–45]. Reactions

15 and 16 correspond to phase oxide formation and electro-oxidation to Fe(III) species. The reversible characteristics of these processes depend strongly on the solution pH. In acid solutions, an irreversible layer associated with the passive state of iron is produced, while in alkaline electrolytes it should be related to the relatively fast $Fe(OH)_2$/FeOOH redox systems [26, 27, 46]. For each solution composition and pH > 4, a complex sandwich-type oxide phase can be formed. The time-dependent formation of three-dimensional porous oxide layers on the iron electrode surface at pH > 4.2 causes instability of the system. The three-dimensional oxide layers contain Fe(III) species [5, 47].

The electroreductions of the different iron oxides are remarkably different, and have been systematically and thoroughly studied by different authors [14, 16, 48–57]. In any case, the more remarkable characteristics of the overall process are the gradual deprotonation and the progressive dehydration of the anodic product layer along the increasing potential. The latter process is more effective at low pH and when the length of time related to the formation of the anodic product increases. The duplex structure of the anodic oxide film on iron in neutral solutions was recognized a long time ago [58–64]. At pH 8.4, the complex structure consisting of anhydrous oxide as an inner layer and hydrated oxide as an outer layer has been proposed on the basis of cathodic reduction experiments combined with ellipsometry [8, 9, 33, 65, 66].

The reaction pathway implies dynamic characteristics for the overall interphase, namely, on the dissolving metal plane and on the structure of the oxygen-containing layer, whether it has a constant thickness at each fixed potential or its thickness increases during the electrodissolution process. This dynamic character is revealed through the ageing of the different surface species and bulk oxide phases formed during the anodic process. These ideas are supported in part by Auger analysis of the composition–depth profile of the anodic oxide film [65] and, to a great extent, are assumed through the potential-dependent relaxation of the surface in the mechanism used by Schweickert *et al.* to interpret the impedance measurements of the anodic dissolution on iron [12].

5. Conclusions

The potentiodynamic response of iron in dilute acid and neutral aqueous electrolytes to fast perturbations applied in the potential range for anodic dissolution of the metal and formation of passivating layers, despite depending on the solution pH, can be coherently interpreted through a reaction pathway which takes into account the dynamic characteristics both of the metal surface and of the structure of the pre-passivating and passivating oxygen-containing films. The reaction scheme is based upon charge transfer processes coupled to deprotonation processes, and ageing, dehydration and topochemical reactions. Earlier mechanistic interpretations are formally included in the reaction pathway postulated in the present work.

Acknowledgements

INIFTA is sponsored by the Consejo Nacional de Investigaciones Científicas y Técnicas, the Universidad Nacional de La Plata and the Comisión de Investigaciones Científicas (Provincia de Buenos Aires). This work was partially sponsored by the SENID (Navy Research and Development Service of Argentina) and the Regional Program for the Scientific and Technological Development of the Organization of the American States.

References

[1] M. Fisher, *Werkstoffe u. Korros.* **29** (1978) 188.
[2] *Idem, Z. Phys. Chem.* **260** (1979) 93.
[3] *Idem, ibid* **260** (1979) 121.
[4] D. B. Gibbs and M. Cohen, *J. Electrochem. Soc.* **119** (1972) 416.
[5] N. Sato and T. Notoya, *Denki Kagaku* **35** (1967) 100.
[6] T. Noda, K. Kudo and N. Sato, *J. Japan Inst. Metals* **37** (1973) 951.
[7] R. Nishimura, K. Kudo and N. Sato, *Surf. Sci.* **96** (1980) 413.
[8] B. S. Pak, W. Paik and I. H. Yeo, *J. Korean Chem. Soc.* **22** (1978) 365.
[9] A. G. Akimov, N. P. Andreeva and I. L. Rozenfeld, *Elektrokhim.* **15** (1979) 1888.
[10] J. R. Vilche and W. J. Lorenz, *Corros. Sci.* **12** (1972) 785.
[11] J. Bessone, L. Karakaya, P. Lorbeer and W. J. Lorenz, *Electrochim. Acta* **22** (1977) 1147.
[12] H. Schweickert, W. J. Lorenz and H. Friedburg, *J. Electrochem. Soc.* **127** (1980) 1693.
[13] K. Ogura and H. Wada, *Electrochim. Acta* **25** (1980) 913.

[14] J. V. Dobson, T. Dickinson and P. R. Snodin, *J. Electroanal. Chem.* 88 (1978) 363.
[15] S. Sklarska-Smialowska and G. Mrowczynski, *Brit. Corros. J.* **10** (1975) 187.
[16] J. M. Lecuire, *J. Electroanal. Chem.* **66** (1975) 195.
[17] K. E. Heusler, *Z. Elektrochem.* **62** (1958) 582.
[18] J. O'M. Bockris, D. Drazic and A. R. Despic, *Electrochem. Acta* **4** (1961) 325.
[19] J. J. Podestá and A. J. Arvía, *ibid* **10** (1965) 171.
[20] E. J. Kelly, *J. Electrochem. Soc.* **115** (1968) 1111.
[21] F. Hilbert, Y. Miyoshi, G. Eichkorn and W. J. Lorenz, *ibid* **118** (1971) 1919.
[22] I. Epelboin, C. Gabrielli, M. Keddam and H. Takenouti, *Electrochim. Acta* **20** (1975) 913.
[23] G. Pinard-Legry and G. Plante, *Mater. Chem.* **1** (1976) 321.
[24] G. Bech-Nielsen, *Electrochim. Acta* **21** (1976) 627.
[25] J. R. Vilche and A. J. Arvía, *Anal. Acad. Cs. Ex. Fis. Nat. Buenos Aires*, in press.
[26] R. S. Schrebler Guzmán, J. R. Vilche and A. J. Arvía, *Electrochim. Acta* (in press).
[27] J. R. Vilche and A. J. Arvía, *Proc. 7th Int. Congr. Met. Corros., Rio de Janeiro* (1978) p. 245 (publ. 1979).
[28] R. S. Schrebler Guzmán, J. R. Vilche and A. J. Arvía, *J. Appl. Electrochem.* **11** (1981) 000.
[29] B. E. Conway, H. Angerstein-Kozlowska, F. C. Ho, J. Klinger, B. MacDougall and S. Gottesfeld, *Faraday Disc. Chem. Soc.* **56** (1973) 210.
[30] R. S. Schrebler Guzmán, J. R. Vilche and A. J. Arvía, *J. Appl. Electrochem.* 9 (1979) 321.
[31] R. N. O'Brien and K. V. N. Rao, *J. Electrochem. Soc.* **112** (1965) 1245.
[32] T. R. Jayaraman, V. K. Venkatesan and H. V. K. Udupa, *Electrochim. Acta* **20** (1975) 209.
[33] M. Cohen, D. Mitchell and K. Hashimoto, *J. Electrochem. Soc.* **126** (1979) 442.
[34] J. R. Vilche and A. J. Arvía, *Acta Cient. Venezuela*, in press.
[35] N. R. Tacconi, J. O. Zerbino and A. J. Arvía, *J. Electroanal. Chem.* 79 (1977) 287.
[36] J. O. Zerbino, N. R. Tacconi, A. Calandra and A. J. Arvía, *J. Electrochem. Soc.* **124** (1977) 475.
[37] R. V. Moshtev, *Electrochim. Acta* **15** (1970) 657.
[38] F. M. Delnick and N. Hackerman, in 'Passivity of Metals' (edited by R. P. Frankenthal and J. Kruger) The Electrochemical Society, Princeton (1978) p. 116.
[39] N. Sata, K. Kudo and R. Nishimura, *J. Electrochem. Soc.* **123** (1976) 1419.
[40] J. L. Ord and D. J. DeSmet, *ibid* **123** (1976) 1876.
[41] T. Tsuru and S. Haruyama, *Corros. Sci.* **16** (1976) 623.
[42] F. C. Ho and J. L. Ord, *J. Electrochem Soc.* **119** (1972) 139.
[43] F. Zucchi, G. Brunoro, G. Trabanelli and M. Zucchini, *Surf. Techol.* 4 (1976) 497.
[44] F. M. Delnick and N. Hackerman, *J. Electrochem. Soc.* **126** (1979) 732.
[45] M. Froelicher, M. Maja and P. Spinelli, *31st ISE Meeting, Venice* (1980) p. 804.
[46] V. A. Macagno, J. R. Vilche and A. J. Arvía, *J. Appl. Electrochem.* **11** (1981) 417.
[47] P. Lorbeer and W. J. Lorenz, *Electrochim. Acta* **25** (1980) 375.
[48] A. Hickling, *Electrochim. Acta* **18** (1973) 635.
[49] K. Ogura, *J. Electroanal. Chem.* **79** (1977) 149.
[50] K. Ogura and T. Majima, *Electrochim. Acta* **23** (1978) 1361.
[51] K. Ogura and H. Wada, *ibid* **25** (1980) 913.
[52] P. D. Allen, N. A. Hampson and G. J. Bignold, *J. Electroanal. Chem.* **99** (1979) 299.
[53] *Idem, Ibid* **111** (1980) 223.
[54] J. M. Lecuire, *Analysis* **2** (1973) 489.
[55] *Idem, ibid* 2 (1973) 495.
[56] J. M. Lecuire and O. Evrard, *J. Electroanal. Chem.* **78** (1977) 331.
[57] J. M. Lecuire and Y. Pillet, *ibid* **91** (1978) 99.
[58] M. Nagayama and M. Cohen, *J. Electrochem. Soc.* **110** (1963) 670.
[59] N. Sato and M. Cohen, *ibid* **111** (1963) 624.
[60] M. Nagayama and M. Cohen, *ibid* **109** (1962) 781.
[61] V. Markovac and M. Cohen, *ibid* **114** (1967) 674.
[62] N. Sato, K. Kudo and T. Noda, *Corros. Sci.* **10** (1970) 785.
[63] N. Sato, T. Noda and K. Kudo, *Electrochim. Acta* **19** (1974) 471.
[64] T. Misawa, K. Hashimoto and S. Shimodaira, *Corros. Sci.* **14** (1974) 131.
[65] M. Seo, N. Sato, J. B. Lumsden and R. W. Staehle, *ibid* **17** (1977) 209.
[66] J. Kruger and J. P. Calvert, *J. Electrochem. Soc.* **114** (1967) 43.